

# A Catalogue of Potential Adaptive Optics Survey Fields from the UKIRT Archive

N. M. Christopher<sup>1</sup> & Ian Smail<sup>2</sup>

<sup>1</sup> *Department of Physics, Durham University, South Road, Durham, DH1 3LE, UK*

<sup>2</sup> *Institute for Computational Cosmology, Durham University, South Road, Durham, DH1 3LE, UK*

Accepted ... ; Received ... ; in original 2005 August 18

## ABSTRACT

We present a multicolour catalogue of faint galaxies situated close to bright stars,  $V \lesssim 15$ , with the aim of identifying high-redshift galaxies suitable for study with adaptive optics-equipped near-infrared imagers and spectrographs. The catalogue is constructed from archival calibration observations of UKIRT Faint Standard stars with the UFTI camera on UKIRT. We have analysed the deepest 16 fields from the archive to provide a catalogue of galaxies brighter than  $K \sim 20.3$  lying within  $25''$  of the guide stars. We identify 111 objects in a total survey area of 8.7 sq. arcmin, of these 87 are classified as galaxies based on their light profiles in our  $\sim 0.5''$  median seeing  $K$ -band images. Of these, 12 galaxies have  $(J-K) \geq 2.0$  consistent with them lying at high-redshifts,  $z \gtrsim 2$ . These 12 very red galaxies have  $K$ -band magnitudes of  $K = 18.1\text{--}20.1$  and separations from the guide stars of  $4\text{--}20''$  and hence are very well-suited to adaptive optics studies to investigate their morphologies and spectral properties on sub-kpc scales. We provide coordinates and  $JHK$  photometry for all catalogued objects.

**Key words:** galaxies: – infrared: galaxies – galaxies: evolution – galaxies: high-redshift – galaxies: photometry

## 1 INTRODUCTION

The high-resolution optical and near-infrared imaging from *Hubble Space Telescope* (*HST*) has provided unique insights into the morphological evolution of galaxies in the restframe optical over the  $\sim 8$  Gyrs to  $z \sim 1$  (e.g. Glazebrook et al. 1995; Giavalisco et al. 2004; Thompson et al. 2001). However, the warm thermal environment of *HST* precludes sensitive imaging at wavelengths beyond  $\sim 1.5\mu\text{m}$  (the middle of the  $H$ -band). This means that *HST* cannot track the restframe optical morphologies of galaxies much past  $z \sim 1\text{--}1.5$  and has to rely on imaging their restframe UV emission – a spectral region much more sensitive to recent star formation and the influences of dust.

Fortunately, adaptive optics (AO) systems operating in the near-infrared waveband on large ground-based telescopes can be used to compliment the optical view provided by *HST* with comparable (or better) spatial resolution:  $\lesssim 0.1\text{--}0.2$  arcsec on faint galaxies (Larkin et al. 2001; Glassman et al. 2002; Cresci et al. 2005). These ground-based AO systems also provide the exciting opportunity to obtain very high angular resolution spectroscopy of these galaxies, necessary to study their kinematics on kpc scales (e.g. Eisenhauer et al., 2003). The drawback with such studies is the need for a bright nearby star to provide a suitable reference source for

wavefront correction to remove the blurring caused by the atmosphere. For typical AO systems the guide star must be brighter than  $V \sim 14$  and situated within  $\sim 20$  arcsec for it to provide any measurable improvement to the achieved image quality (Le Louarn et al. 1998; Doel et al. 2000; Benn 2001). However, some correction can be achieved with fainter guide stars or larger separations if these are supplemented by information about the atmospheric phase transmission from an additional artificial laser guide star.

The restriction on AO studies of faint galaxies is thus the need to have a suitable bright guide star within the field. This requirement severely limits the number of suitable targets and has resulted in adaptive optics studies so far having had relatively limited impact on the study of faint galaxies, although the recent commissioning of laser guide star capabilities on several 8–10-m class telescopes (e.g. Minowa et al. 2005) may change this. To provide target fields suitable for natural guide star studies, two groups have published catalogues of galaxies identified close to bright stars: Larkin & Glassman (1999) and Baker et al. (2003).

Larkin & Glassman provided  $K$ -band (and some  $J$ -/ $H$ -band photometry) for around 40 galaxies to a  $5\text{-}\sigma$  limit of  $K \sim 20$  in 5 patches close to  $R = 8.5\text{--}10.3$  bright stars in the Northern hemisphere. Due to the need to place the stars in one corner of the array (to limit the effects of charge bleed-

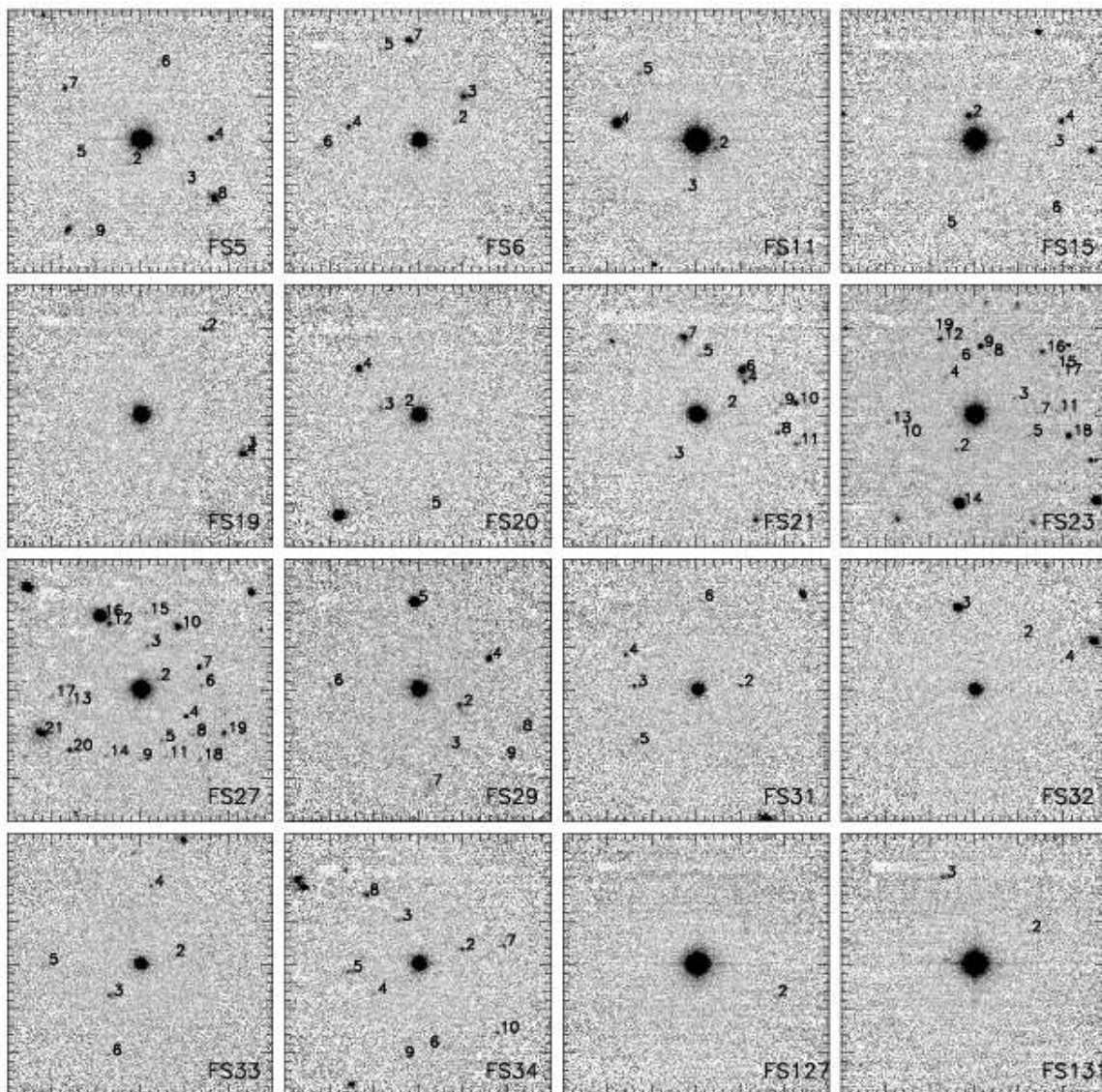


**Figure 1.** The central  $60'' \times 60''$  region of the  $K$ -band images of the 16 fields in our sample. We identify the other objects in the fields using the numbering scheme from Table 2. Each panel is centred on the faint standard in the field and has North top and East to the left. The major tick marks on the axes are every  $10''$ .

ing), all but  $\sim 15$  of these galaxies are beyond 25-arcsec from the correction star, beyond which the corrections provided by typical AO systems using a single star become negligible. In contrast, Baker et al. (2003) imaged regions around 42  $R = 9.0$ – $12.4$  guide stars in the Southern Hemisphere in just the  $K$ -band to a  $5\text{-}\sigma$  limit of  $K \sim 19.5$ . They find around 350 galaxies within 25 arcsec of the guide stars.

Both of these previous studies have used targeted observations to construct catalogues of sources around bright stars. Larkin & Glassman (1999) used 4 nights on the Keck telescope and the NTT took 6 nights to complete the Baker et al. (2003) study. However, there are opportunities of obtaining comparably deep data for free from calibration fields on ground- (and indeed space-based) telescopes, by exploiting archives now available for most major facilities.

Our study focuses on the archive for one telescope which is particularly well-suited to this programme: the UK In-

frared Telescope (UKIRT).<sup>\*</sup> UKIRT operates exclusively in the near- and mid-infrared – the preferred spectral region for ground-based AO studies of high-redshift galaxies. The telescope also has a fully-integrated data reduction pipeline associated with the primary science instruments on the telescope and hence the reduction of data from the archive can exploit the same pipeline to efficiently process the large quantities of data necessary for the project. The bulk of the photometric calibration for the UKIRT imaging cameras also relies on a small number of standard stars – the UKIRT Faint Standards (FS) from Hawarden et al. (2001). The UKIRT FS list is ideal as the stars in the primary list are predominantly equatorial and typically bright enough (but

<sup>\*</sup> The United Kingdom Infrared Telescope (UKIRT) is operated by the Joint Astronomy Centre on behalf of the UK Particle Physics and Astronomy Research Council.

not too bright) to use as AO guide stars. The majority of the recent imaging data are taken with a single instrument, UFTI, guaranteeing it is homogeneous. There are approximately 140hrs of observations of faint standard stars in the *JHK* filters with UFTI in the UKIRT archive. The majority of these observations are of the primary standard list from Hawarden et al. (2001). This means we can expect the cumulative integration on many of the calibration fields to reach the depths necessary for studying the morphologies of  $z \gtrsim 1$  galaxies, i.e.  $K \sim 20$ .

We have therefore searched the UKIRT Archive for suitable FS fields, reduced, calibrated and catalogued these to provide a list of faint galaxies suitable for studies with current adaptive optics imagers and spectrographs. This paper is structured as follows: in §2 we detail the field selection and the reduction of the data. In §3 we describe the analysis of these fields and discuss the properties of the sources we detect. Finally, in §4 we give our conclusions.

## 2 OBSERVATIONS & REDUCTION

The first step in our study was to query the UKIRT Archive<sup>†</sup> for all the observations in the *JHK*-bands with the UFTI camera (Roche et al. 2002) of stars in the extended UKIRT Faint Standard List (Hawarden et al. 2001). We then select all those with potentially more than 2.5-ks integration in the *K*-band and available in archive as of 2005 August 1st. We removed any FS with  $V \gtrsim 15$  (the deepest likely limit for a natural guide star with present AO systems) and those with reddening in the field of  $A_K \geq 0.02$  ( $A_V > 0.2$ ) based on Schlegel et al. (1998) as estimated from NED.<sup>‡</sup>

From the initial 83 faint standards (28 from the primary list, those with IDs < 40, and 55 from the extended list, those with IDs > 100) this leaves us with 17 fields. We discard one field, FS 16, due to the combination of shallow depth and poorer than average image quality – leaving 16. We list the IDs, coordinates and total exposure times in the *J*-, *H*- and *K*-bands for these fields in Table 1.

Observations of standards taken with UFTI typically jitter the star around the lower-right-hand quadrant of the HAWAII-1 detector and only read-out this  $512 \times 512$  pixel region. At the nominal pixel scale of UFTI,  $0.0908 \text{ arcsec pixel}^{-1}$ , this field corresponds to  $\sim 46''$  – well matched to the isoplanatic patch in the near-infrared. The standard calibration sequence consists of a dark exposure, followed by 5 exposures of the standard in a diagonal cross pattern.

Data are reduced using the ORACDR pipeline for UFTI data (Economou et al. 2004). Due to the development of the pipeline and changes in the file header parameters, slightly different incantations are needed for data taken on different dates. Prior to 2000 August 1 we used the ORACDR\_UFTI\_OLD setup from the STARLINK v.2004.2 release, once the .FIT file

extensions are renamed to .FITS this automatically processes the data, subtracting suitable dark frames, creating and applying a filter-dependent flat field (using the data themselves) and aligning the frames from the positions of objects within the fields (or if there are insufficient of these to reliably define a transformation then the telescope offsets written in the frame headers are used instead), before co-adding them to create a final image. After 2000 August 1 we use the ORACDR\_UFTI setup after applying the FITS2NDF command from the STARLINK CONVERT package to convert the FITS files into a merged NDF format file (between 2001 January 1 and approximately 2001 November 16 we first require to rename the .FIT file extensions). The ORACDR pipeline is then identical to that run on the earlier data. For the most part the pipeline reduces the observations with no intervention using the reduction recipes given in the headers of the data frames.

The co-added frames from each of the jitter sets in a given filter of a particular star were then combined together using STARLINK CCDPACK routines to give a final frame in each of the *J*-, *H*- and *K*-bands for each standard star field. Due to the removal of poor quality data and problems retrieving data from the archive from particular nights, the cumulative exposure times for some fields are slightly below those initially anticipated (Table 1).

In total, data were retrieved for the selected standard stars from over 360 nights from 1999 to 2004, with around 10,000 individual frames retrieved and processed.

## 3 ANALYSIS & DISCUSSION

The mean exposure times for the 16 FS in our final sample are 3.2 ks, 1.7 ks and 3.7 ks in *J*-, *H*- and *K*-band respectively. This is sufficient to reach  $5\text{-}\sigma$  point-source limits of  $J \sim 21.4$ ,  $H \sim 20.3$  and  $K \sim 20.3$  – adequate to detect  $L^*$  galaxies at  $z \sim 1$  and beyond. The median seeing in the *K*-band images is  $0.57''$  as measured from the FS themselves. The FWHM for each stacked *K*-band image is reported in Table 1. The median FWHM in the *J*- and *H*-bands is  $0.70''$  and  $0.67''$  respectively. As these are measured from the co-added images resulting from observations spread over 5 years these values can be taken to represent firm upper limits on the typical seeing achieved by UKIRT.

### 3.1 Galaxy Catalogues

Catalogues were constructed from the *K*-band frames, after trimming these to a  $60'' \times 60''$  region centred on the FS. To construct our catalogues we use SExtractor (Bertin & Arnouts 1996) within GAIA. The frames were convolved with a Gaussian kernel with a FWHM comparable to the seeing, before objects were identified using a minimum area of 9 pixels each above a threshold of  $1\text{-}\sigma$  of the sky variance. Catalogues were visually inspected and cleaned of a small number of faint spurious features.

For our sample we select only those objects with  $2''$ -diameter aperture magnitudes brighter than the  $5\text{-}\sigma$  limiting *K*-band magnitudes listed in Table 1. These magnitude limits were determined from the fluctuations in  $2''$ -diameter apertures randomly placed on blank sky regions within the frames. These estimates suggested that the typical  $5\text{-}\sigma$  depth

<sup>†</sup> The UKIRT Archive is provided through the UK Astronomy Data Centre, [http://archive.ast.cam.ac.uk/ukirt\\_arch](http://archive.ast.cam.ac.uk/ukirt_arch)

<sup>‡</sup> The NASA/IPAC Extragalactic Database (NED) is operated by the Jet Propulsion Laboratory, California Institute of Technology, under contract with the National Aeronautics and Space Administration.

**Table 1.** Log of the observations of Faint Standards in the UKIRT Archive. We list the ID,  $K$ - and  $V$ -band magnitudes for the star, its nominal position, total exposure times for the final stacked  $JHK$  images, the FWHM of the  $K$ -band frame, the  $5\text{-}\sigma$  limiting  $K$ -band magnitude (measured in a  $2''$ -diameter aperture) and the total number of stars and galaxies (excluding the FS) in our catalogues within  $25''$  of the FS and brighter than this limit.

Star	$K$	$V$	R.A.	Dec.	$J$	$T_{\text{Exp}}$	$K$	FWHM $_K$	$K_{\text{lim}}$	N	
			(J2000)			$H$		( $''$ )		Star	Gal.
FS 5	12.34	12.41	01 54 34.65	−06 46 00.4	2450	850	2690	0.57	20.1	1	7
FS 6	13.38	12.80	02 30 16.64	+05 15 51.1	1275	750	3525	0.52	20.4	0	6
FS 11	11.25	11.72	04 52 58.92	−00 14 41.6	1825	785	1775	0.72	19.7	2	2
FS 15	12.35	14.05	08 51 05.81	+11 43 46.9	4625	2130	3655	0.67	20.4	0	5
FS 19	13.78	13.01	10 33 42.75	−11 41 38.3	2375	1725	3525	0.78	20.3	1	2
FS 20	13.50	13.06	11 07 59.93	−05 09 26.1	2200	1300	2350	0.57	20.3	1	3
FS 21	13.15	12.50	11 37 05.15	+29 47 58.4	5300	2800	5275	0.55	20.7	0	10
FS 23	12.38	14.75	13 41 43.57	+28 29 49.5	5750	1905	4795	0.59	20.4	9	9
FS 27	13.13	14.70	16 40 41.56	+36 21 12.4	7050	4025	9250	0.66	20.5	6	14
FS 29	13.31	12.74	21 52 25.36	+02 23 20.7	4950	4800	6425	0.56	20.5	1	7
FS 31	14.04	13.09	23 12 21.60	+10 47 04.1	2100	900	3650	0.54	20.4	1	4
FS 32	13.68	12.96	23 16 12.37	−01 50 34.6	1850	750	2650	0.52	20.3	2	1
FS 33	14.25	13.42	12 57 02.30	+22 01 52.8	2300	1750	3150	0.64	20.5	0	5
FS 34	13.00	12.34	20 42 34.73	−20 04 34.8	2050	775	1575	0.55	20.0	0	9
FS 127	14.20	13.86	10 06 29.03	+41 01 26.6	2315	775	2970	0.64	20.4	0	1
FS 131	11.75	12.56	12 14 25.40	+35 35 55.6	1975	855	2220	0.64	19.8	0	2

of our observations is  $K \sim 20.3$ . We quote aperture  $K$ -band magnitudes for all of our detected sources in Table 2, the median correction from these to "total" magnitudes is  $-0.18 \pm 0.04$  as measured from the bright stars in the fields. We also note that we have applied no reddening corrections to any of the magnitudes in this study due to the low reddening in these fields in the near-infrared. We measure colours for all objects in  $1.0''$ -diameter apertures, sufficient to give representative colours for the typically compact faint galaxies and stars in our sample. These are corrected for the seeing differences between the  $JHK$  frames in each individual fields, as measured from the FS star, with typical aperture corrections of:  $\Delta(J - K) = -0.15$  and  $\Delta(H - K) = -0.11$ . The colours or  $2\text{-}\sigma$  limits listed in Table 2 and used in Figs. 4 & 5 have had these aperture corrections applied.

The total number of objects detected within  $25''$  radius of the FS (excluding the FS itself) and brighter than the  $5\text{-}\sigma$  limits of the respective fields,  $K = 19.7\text{--}20.7$ , are listed in Table 1. Out to  $25''$  over the 16 fields, we cover a surveyed area of 8.7 sq. arcmin and detect 111 objects (excluding the FS) brighter than the  $5\text{-}\sigma$  limits.

Star-galaxy separation is achieved by comparing the magnitudes within apertures of  $2 \times \text{FWHM}$  and  $4 \times \text{FWHM}$  (Reid et al. 1996). This provides a relatively clear differentiation between objects with star-like and non-star light profiles (Fig. 2). The FS stars exhibit a constant offset  $K_{2 \times \text{FWHM}} - K_{4 \times \text{FWHM}} = 0.30 \pm 0.02$ , with extended galaxies having larger offsets. Roughly two-thirds of the sample have  $K_{2 \times \text{FWHM}} - K_{4 \times \text{FWHM}} > 0.40$  which we take as the dividing line in our classification to  $K \leq 19.5$  (Table 2). Fainter than  $K = 19.5$  we have classified all objects as galaxies, unless they have  $K_{2 \times \text{FWHM}} - K_{4 \times \text{FWHM}} \leq 0.40$  and colours consistent with those of the brighter stars in our sample,  $(J - K) \leq 1$  and  $(H - K) \leq 0.6$  (Fig. 4), in which case

they are classed as stars – this effects only 8 objects in our sample. In total we have 24 stars (plus the 16 FS) and 87 galaxies.

We list the properties of the 111 objects and the 16 FS stars in our catalogue in Table 2. The objects in each field are identified by their ranked distance from the FS star and we give their short name, the position,  $K$ -band magnitude in our  $2''$ -diameter aperture ( $J - K$ ) and ( $H - K$ ) aperture colours or limits, star-galaxy classification (S or G) and radial distance from the FS star in arcsec. The astrometry in these images are tied to USNO but due to the limited fields of view the astrometry is not accurate to better than  $0.5''$  rms.<sup>§</sup>

### 3.2 Galaxy Properties

We show the number counts of sources in our fields (excluding the bright stars and the FS stars) in Fig. 3. We compare these to representative counts from the literature (Gardner et al. 1993; Baker et al. 2003) and find good agreement in the overall number of sources we detect and the slope of the differential number counts,  $\alpha \sim 0.3$ . We take this as confirmation that our catalogue is not significantly incomplete above our typical limiting magnitude,  $K \sim 20.3$ .

In Fig. 4 we show the  $(J - K)$ – $(H - K)$  colour-colour diagram for all objects in our fields (including the FS stars). The figure shows that those objects classified as stars on the basis of their light profiles exhibit a tight locus, with relatively blue  $(J - K)$  and  $(H - K)$  colours, consistent with the measured colours of the FS stars. The galaxies have a

<sup>§</sup> If more precise relative positions are required please contact the Authors for the reduced images.

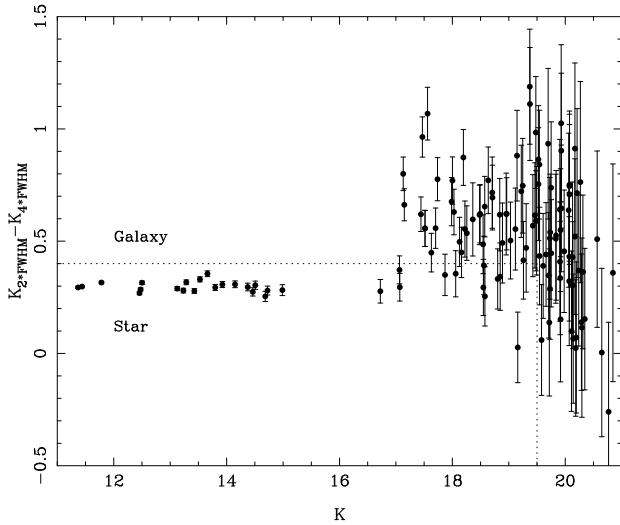


**Figure 2.** Our criteria used for star-galaxy classification, following Reid et al. (1996). We plot the difference between the  $K$ -band magnitudes of all objects measured in apertures with diameters  $2*$  and  $4*$  the FWHM of the FS in that particular field, against their large-aperture  $K$ -band magnitudes. The FS stars, and other bright stars serendipitously detected in these fields, exhibit a constant value for  $K_{2*FWHM} - K_{4*FWHM}$  and we use the mean and scatter for these to determine a dividing line between morphologically-classified stars and galaxies – at  $K_{2*FWHM} - K_{4*FWHM} = 0.40$ . Fainter than  $K = 19.5$  the measured magnitudes lack sufficient precision to reliably determine this classification. Due to the steeply rising galaxy number counts it is expected that the vast majority of sources at  $K \geq 19.5$  will be galaxies and hence we class all objects fainter than this as galaxies, unless they have  $K_{2*FWHM} - K_{4*FWHM} \leq 0.40$  and colours consistent with those of the brighter stars in our sample (Fig. 3).

much broader distribution, extending to redder ( $J - K$ ) and ( $H - K$ ) colours. The reddest galaxies have ( $J - K$ )  $\gtrsim 2$  or ( $H - K$ )  $\gtrsim 1.5$ . We plot tracks showing the variation in colour of galaxies with spectral energy distributions similar to present-day ellipticals and an Scd galaxy. These tracks illustrate that the galaxies with the reddest ( $J - K$ ) colours are likely to lie at high redshifts,  $z \gtrsim 2$  (Franx et al. 2003). We note that we have 12 galaxies with ( $J - K$ )  $\geq 2.0$  brighter than  $K \sim 20.5$ , with 3 galaxies with colours of ( $J - K$ )  $\geq 2.3$ .

Focusing on the 12 ( $J - K$ )  $\geq 2.0$  galaxies, we find that they are all well-resolved with FWHM (corrected for seeing) of  $\sim 1.4''$  ( $\sim 10$  kpc at  $z \sim 2$ ) and have a median magnitude of  $K = 19.0$ . The mean ( $H - K$ ) colour of these galaxies is  $1.3 \pm 0.3$ , consistent with the colours expected for  $z \sim 2$  galaxies. These galaxies are well-situated for AO-assisted studies with a median separation from the FS star of  $13.0''$ . Half of these galaxies are found in just two fields, FS27 and FS34, as expected if they represent a strongly-clustered population of high-redshift galaxies (Daddi et al. 2004).

#### 4 CONCLUSIONS

We have undertaken an archival survey for galaxies close to bright stars which would be suitable for targeting with adap-

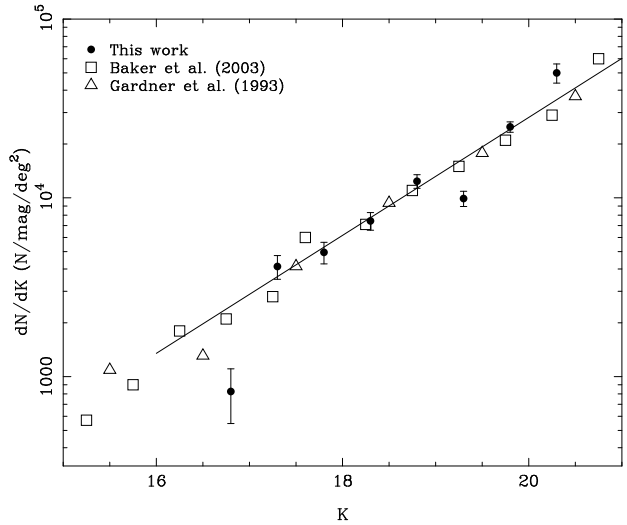


**Figure 3.** The differential number counts as a function of their  $2''$ -diameter aperture magnitudes for sources detected in the  $25''$ -radius regions around the 16 FS stars in our sample. We plot just the faint-end of our counts, excluding the bright FS stars. We correct the number counts for survey area using the  $5\text{-}\sigma$  detection limits for each field from Table 1. The error-bars on our data points are Poisson and so underestimate the likely variance resulting from the clustering of galaxies in our small survey fields. We compare our counts to those from the similar study of Baker et al. (2003) and also from Gardner et al. (1993), showing generally good agreement between the various surveys. We also show the canonical  $\alpha = 0.33$  count slope for  $K$ -band galaxy counts, normalised to fit our data points.

tive optics imagers and spectrographs on 4–8-m class telescopes. Our survey relies on the homogeneous data archive available for the UKIRT telescope and especially the large quantities of high-quality calibration imaging taken with the UFTI near-infrared camera. These images, of stars from the UKIRT Faint Standards List, provide deep  $JHK$  observations of regions covering the isoplanatic patch around 16 optically-bright,  $V \lesssim 15$  stars. By co-adding all of the data available for these 16 stars we survey  $25''$ -radius regions around each star to provide a total area coverage of 8.7 sq. arcmins to a  $5\text{-}\sigma$  depth of  $K \sim 20.3$ .

Disregarding the FS guide stars, we detect 111 objects in the 8.7 sq. arcmin survey region and exploiting the  $\sim 0.5''$  average image quality from our data, we classify these into stars or galaxies on the basis of their light profiles. We find 87 galaxies and 24 stars. The ( $J - K$ )-( $H - K$ ) colour-colour distributions for these objects show that as expected the stars are typically bluer in both ( $J - K$ ) and ( $H - K$ ) than the galaxies. Moreover, we identify 12 galaxies whose ( $J - K$ ) colours exceed ( $J - K$ ) = 2.0, consistent with these being high-redshift galaxies. These galaxies have  $K$ -band magnitudes of  $K = 18.1\text{--}20.1$  and separations from the FS guide star of  $4\text{--}20''$  and hence are very well-suited to AO studies to investigate their morphologies and spectral properties on sub-kpc scales.

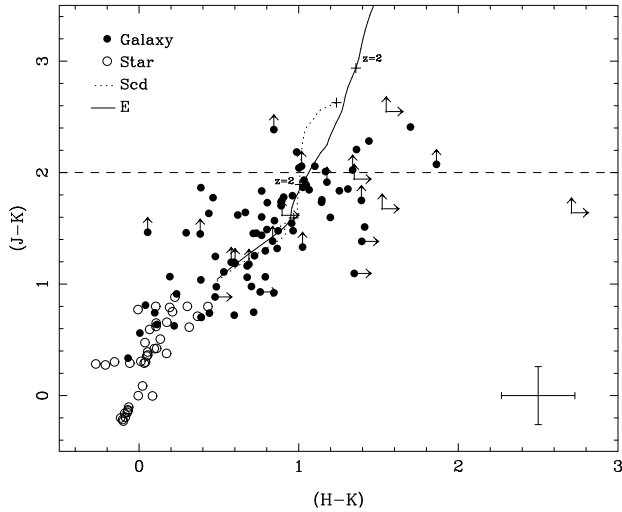


**Figure 4.** A plot of the distribution of  $(J - K)$  and  $(H - K)$  colours for galaxies and stars in our catalogue. Galaxies and stars are distinguished by their symbols and we plot  $2\text{-}\sigma$  lower limits where there is no formal detection in the  $J$ - or  $H$ -bands. The stars show a tight locus and are generally bluer in both  $(J - K)$  and  $(H - K)$  than the galaxies, which have a broader colour distribution. We plot two tracks showing the variation in apparent colour for galaxies with spectral energy distributions comparable to present-day ellipticals or Scd galaxies (we have shifted both tracks by  $\Delta H = 0.2$  to account for calibration uncertainties between the models and observations). These start with blue  $(J - K)$  and  $(H - K)$  colours at  $z = 0$  and become increasingly red at higher redshifts, the tracks extend to  $z = 3$  and we identify the point corresponding to  $z = 2$  on both tracks. The distribution of galaxy colours broadly spans that expected for passive or star-forming galaxies at  $z \sim 0\text{--}2$ . The dividing line at  $(J - K) = 2$  roughly corresponds to galaxies at  $z \gtrsim 2$  as first noted by Franx et al. (2003). We show the median errors for the colours of our objects in the lower-right-hand corner.

## Acknowledgments

We thank Malcolm Currie, Brad Cavanagh, Peter Draper, Jim Lewis, Nigel Metcalfe and Mark Swinbank for help. This paper uses data taken with UKIRT and retrieved from the UKIRT Archive operated by the UK Astronomical Data Centre. NMC acknowledges support from a Summer Studentship at Durham University. IRS acknowledges support from the Royal Society.

## REFERENCES

- Baker, A.J., et al., 2003, *A&A*,  
 Benn, C.R., 2001, *NewAR*, 45, 59  
 Bertin, E., Arnouts, S., 1996, *A&AS*, 117, 393  
 Cresci, G., Davies, R.I., Baker, A.J., Lehnert, M.D., 2005, *A&A*, 438, 757  
 Daddi, E., Rottgering, H.J.A., Labbe, I., Rudnick, G., Franx, M., Moorwood, A.F.M., Rix, H.W., van der Werf, P.P., van Dokkum, P.G., 2003, *ApJ*, 588, 50  
 Doel, A.P., Dunlop, C.N., Buscher, D.F., Myers, R.M., Sharples, R.M., Major, J.V., 2000, *NewA*, 5, 223  
 Economou, F., Jenness, T., Currie, M.M., Adamson, A.J., Allan, A., Cavanagh, B., 2004, *Starlink User Note* 230.6  
 Eisenhauser, F., et al., 2003, *SPIE 4841, Instrument Design and*

- Performance for Optical/IR Ground-Based Telescopes*, eds. M Iye. & A.F. Moorwood p1548  
 Franx, M., et al., 2003, *ApJ*, 587, L79  
 Gardner, J.P., Cowie, L.L., Wainscoat, R.J., 1993, *ApJ*, 415, L9  
 Giavalisco, M., et al., 2004, *ApJ*, 600, L93  
 Glassman, T.M., Larkin, J.E., Lafreniere, D., 2002, *ApJ*, 581, 865  
 Glazebrook, K., Ellis, R.S., Santiago, B., Griffiths, R., 1995, *MNRAS*, 275, L19  
 Hawarden, T., et al., 2001, *MNRAS*, 325, 563  
 Larkin, J.E., Glassman, T.M., 1999, *PASP*, 111, 1410  
 Larkin, J.E., Glassman, T.M., Wizinowich, P., Acton, D.S., Lai, O., Filippenko, A.V., Coil, A.L., Matheson, T., 2001, *PASP*, 112, 1526  
 Le Louarn, M., Foy, R., Hubin, N., Tallon, M., 1998, *MNRAS*, 295, 756  
 Minowa, Y., et al., 2005, *ApJ*, 629, 29  
 Reid, I.N., Yan, L., Majewski, S., Thompson, I., Smail, I., 1996, *AJ*, 112, 1472  
 Roche P.F., et al., 2002, *Proc. SPIE 4841, Instrument Design and Performance for Optical/IR Ground-Based Telescopes*, eds. M Iye. & A.F. Moorwood  
 Schlegel, D.J., Finkbeiner, D.P., Davis, M., 1998, *ApJ*, 500, 525  
 Thompson, R.I., Weymann, R.J., Storrie-Lombardi, L.J., 2001, *ApJ*, 546, 694

**Table 2.** Catalogue of objects in FS fields.

ID	R.A. (J2000)	Dec.	$K_{ap}$	$(J - K)$	$(H - K)$	Class	$r$ ( $''$ )
FS5-1	01 54 34.587	-06 45 59.21	12.51±0.01	0.00±0.01	-0.01±0.01	S	0.0
FS5-2	01 54 34.758	-06 46 04.14	19.72±0.20	≥2.06	1.02±0.44	G	6.1
FS5-3	01 54 33.961	-06 46 08.53	19.56±0.18	1.55±0.39	0.96±0.44	G	13.6
FS5-4	01 54 33.567	-06 45 59.48	16.76±0.04	0.00±0.05	0.08±0.06	S	15.8
FS5-5	01 54 35.578	-06 46 02.20	19.98±0.23	≥1.62	≥0.90	G	15.9
FS5-6	01 54 34.284	-06 45 43.21	20.03±0.24	1.87±0.49	0.39±0.35	G	17.2
FS5-7	01 54 35.658	-06 45 47.21	18.33±0.09	1.60±0.21	0.77±0.18	G	20.9
FS5-8	01 54 33.566	-06 46 12.73	17.27±0.05	1.44±0.13	0.77±0.12	G	21.1
FS5-9	01 54 35.356	-06 46 19.52	19.77±0.21	1.38±0.38	≥1.39	G	24.5
FS6-1	02 30 16.641	05 15 50.71	13.53±0.01	-0.13±0.01	-0.07±0.01	S	0.0
FS6-2	02 30 16.104	05 15 54.83	19.93±0.21	1.63±0.52	0.44±0.45	G	9.0
FS6-3	02 30 15.972	05 16 00.66	18.02±0.07	1.64±0.21	0.67±0.18	G	14.1
FS6-4	02 30 17.711	05 15 53.69	18.61±0.10	1.85±0.29	1.31±0.35	G	16.3
FS6-5	02 30 17.227	05 16 11.51	20.34±0.27	≥1.46	0.05±0.48	G	22.6
FS6-6	02 30 18.151	05 15 49.26	19.43±0.15	0.89±0.38	≥0.48	G	22.6
FS6-7	02 30 16.792	05 16 13.55	17.46±0.06	0.46±0.14	0.71±0.12	G	22.9
FS11-1	04 52 58.863	-00 14 41.08	11.48±0.00	0.09±0.01	0.02±0.01	S	0.0
FS11-2	04 52 58.585	-00 14 42.71	18.21±0.10	≥2.55	≥1.55	G	4.5
FS11-3	04 52 59.050	-00 14 52.06	19.70±0.24	0.80±0.32	0.10±0.26	S	12.0
FS11-4	04 53 00.058	-00 14 37.34	14.78±0.02	0.79±0.03	0.19±0.02	S	18.5
FS11-5	04 52 59.721	-00 14 26.47	18.70±0.13	2.18±0.41	0.99±0.25	G	20.1
FS15-1	08 51 05.793	11 43 47.40	12.53±0.01	0.39±0.01	0.05±0.01	S	0.0
FS15-2	08 51 05.886	11 43 52.88	17.78±0.07	1.20±0.14	0.60±0.11	G	5.7
FS15-3	08 51 04.626	11 43 45.98	19.73±0.18	1.93±0.48	1.03±0.35	G	17.1
FS15-4	08 51 04.461	11 43 51.76	18.31±0.09	1.78±0.22	0.91±0.16	G	20.0
FS15-5	08 51 06.284	11 43 27.45	20.36±0.26	≥1.45	0.38±0.41	G	21.2
FS15-6	08 51 04.671	11 43 30.89	19.98±0.21	1.78±0.56	0.46±0.36	G	23.3
FS19-1	10 33 42.772	-11 41 38.32	14.08±0.01	-0.20±0.02	-0.12±0.01	S	0.0
FS19-2	10 33 41.807	-11 41 18.79	18.66±0.10	0.71±0.17	0.37±0.15	S	24.1
FS19-3	10 33 41.203	-11 41 45.82	19.62±0.17	0.70±0.13	0.39±0.11	G	24.2
FS19-4	10 33 41.206	-11 41 47.32	17.83±0.06	0.70±0.13	0.39±0.11	G	24.7
FS20-1	11 07 59.958	-05 09 26.43	13.70±0.01	-0.10±0.01	-0.06±0.01	S	0.0
FS20-2	11 08 00.230	-05 09 24.32	20.25±0.28	≥1.33	1.02±0.60	G	4.6
FS20-3	11 08 00.535	-05 09 25.07	19.34±0.16	2.01±0.45	1.17±0.35	G	8.8
FS20-4	11 08 00.865	-05 09 15.79	17.10±0.05	0.88±0.08	0.22±0.07	S	17.3
FS20-5	11 07 59.824	-05 09 47.64	20.26±0.29	1.18±10.01	0.69±0.63	G	21.4
FS21-1	11 37 05.102	29 47 58.37	13.31±0.01	-0.16±0.01	-0.09±0.01	S	0.0
FS21-2	11 37 04.632	29 48 00.19	20.40±0.27	≥1.39	0.84±0.54	G	6.3
FS21-3	11 37 05.559	29 47 48.45	20.09±0.23	≥2.02	1.34±0.47	G	11.6
FS21-4	11 37 04.282	29 48 05.80	18.79±0.11	1.89±0.32	1.05±0.23	G	13.0
FS21-5	11 37 05.051	29 48 11.87	19.68±0.18	≥2.39	0.84±0.31	G	13.5
FS21-6	11 37 04.316	29 48 08.38	17.59±0.06	1.25±0.16	0.72±0.13	G	14.3
FS21-7	11 37 05.329	29 48 15.93	17.85±0.07	1.48±0.18	0.87±0.14	G	17.8
FS21-8	11 37 03.698	29 47 54.10	19.11±0.13	1.48±0.28	0.96±0.24	G	18.7
FS21-9	11 37 03.640	29 48 00.78	19.59±0.17	1.73±0.43	0.80±0.31	G	19.1
FS21-10	11 37 03.389	29 48 00.94	18.57±0.10	1.70±0.25	0.89±0.19	G	22.4
FS21-11	11 37 03.375	29 47 51.54	19.37±0.15	1.85±0.42	1.07±0.33	G	23.4
FS23-1	13 41 43.626	28 29 51.47	12.54±0.01	0.59±0.01	0.07±0.01	S	0.0
FS23-2	13 41 43.959	28 29 43.48	19.16±0.14	1.84±0.40	0.77±0.28	G	9.1
FS23-3	13 41 42.926	28 29 55.22	20.18±0.25	0.27±0.32	-0.21±0.29	S	9.7
FS23-4	13 41 44.110	28 30 00.28	20.07±0.23	0.61±0.34	0.31±0.33	S	10.8
FS23-5	13 41 42.698	28 29 46.71	20.12±0.24	0.51±0.31	0.13±0.28	S	13.2
FS23-6	13 41 43.922	28 30 04.27	20.37±0.28	0.75±0.52	0.72±0.59	G	13.2
FS23-7	13 41 42.557	28 29 51.71	19.89±0.21	0.56±0.32	0.00±0.28	G	13.9
FS23-8	13 41 43.345	28 30 05.20	20.44±0.29	≥1.20	0.58±0.53	G	14.0
FS23-9	13 41 43.501	28 30 07.12	17.92±0.07	0.31±0.11	0.01±0.10	S	15.6
FS23-10	13 41 44.967	28 29 46.80	20.40±0.28	0.36±0.38	0.05±0.36	S	18.1
FS23-11	13 41 42.230	28 29 52.22	19.82±0.20	0.62±0.35	0.22±0.33	G	18.2
FS23-12	13 41 44.196	28 30 08.94	18.21±0.08	1.75±0.22	0.89±0.16	G	19.0
FS23-13	13 41 45.121	28 29 49.74	20.04±0.22	0.28±0.30	-0.27±0.27	S	19.7
FS23-14	13 41 43.937	28 29 31.04	14.55±0.01	0.47±0.02	0.04±0.02	S	20.7
FS23-15	13 41 42.253	28 30 02.52	20.07±0.23	1.46±0.56	0.30±0.40	G	20.8
FS23-16	13 41 42.440	28 30 05.79	18.08±0.08	0.30±0.12	-0.15±0.11	S	20.9
FS23-17	13 41 42.173	28 30 00.78	20.42±0.28	0.91±0.48	0.23±0.42	G	21.0
FS23-18	13 41 42.010	28 29 46.49	17.11±0.05	0.29±0.07	-0.06±0.07	S	21.7

Table 2. cont.

ID	R.A. (J2000)	Dec.	$K_{ap}$	$(J - K)$	$(H - K)$	Class	$r$ ( $''$ )
FS27-1	16 40 41.615	36 21 13.23	13.31±0.01	0.35±0.01	0.05±0.01	S	0.0
FS27-2	16 40 41.306	36 21 15.50	19.94±0.19	1.16±0.40	0.66±0.40	G	4.2
FS27-3	16 40 41.499	36 21 23.23	19.67±0.17	1.46±0.38	0.73±0.29	G	10.0
FS27-4	16 40 40.771	36 21 06.97	19.07±0.12	0.80±0.19	0.43±0.17	S	11.9
FS27-5	16 40 41.224	36 21 01.40	19.93±0.19	1.32±0.38	0.86±0.32	G	12.7
FS27-6	16 40 40.475	36 21 14.11	20.13±0.22	≥2.07	1.86±0.52	G	13.7
FS27-7	16 40 40.524	36 21 18.33	18.65±0.10	0.38±0.15	0.17±0.14	S	14.0
FS27-8	16 40 40.633	36 21 02.73	20.14±0.22	≥1.68	≥1.52	G	15.8
FS27-9	16 40 41.650	36 20 57.14	20.09±0.21	2.04±0.63	1.00±0.42	G	16.1
FS27-10	16 40 40.922	36 21 27.54	17.90±0.07	1.87±0.19	1.03±0.13	G	16.4
FS27-11	16 40 41.148	36 20 57.67	20.38±0.25	0.74±0.45	0.10±0.37	G	16.5
FS27-12	16 40 42.199	36 21 28.34	18.59±0.10	2.28±0.35	1.44±0.35	G	16.6
FS27-13	16 40 42.975	36 21 09.96	19.38±0.15	0.98±0.35	0.70±0.32	G	16.8
FS27-14	16 40 42.268	36 20 57.96	20.49±0.26	1.04±0.42	0.39±0.34	G	17.2
FS27-15	16 40 41.519	36 21 30.55	19.71±0.17	0.64±0.29	0.11±0.24	G	17.2
FS27-16	16 40 42.377	36 21 30.12	14.53±0.01	0.75±0.02	0.21±0.02	S	19.2
FS27-17	16 40 43.277	36 21 11.65	19.98±0.20	1.30±0.43	0.79±0.36	G	20.1
FS27-18	16 40 40.510	36 20 57.15	20.38±0.25	0.66±0.40	0.17±0.35	S	20.9
FS27-19	16 40 40.057	36 21 03.21	18.69±0.10	0.42±0.16	0.09±0.14	S	21.2
FS27-20	16 40 42.954	36 20 59.29	18.95±0.12	0.42±0.18	0.11±0.16	S	21.4
FS27-21	16 40 43.490	36 21 03.28	17.40±0.06	1.74±0.15	0.89±0.11	G	24.8
FS29-1	21 52 25.358	02 23 19.34	13.45±0.01	−0.14±0.01	−0.07±0.01	S	0.0
FS29-2	21 52 24.740	02 23 15.60	18.81±0.11	1.49±0.27	0.80±0.20	G	9.9
FS29-3	21 52 24.933	02 23 05.94	20.40±0.27	0.74±0.42	0.44±0.37	G	14.8
FS29-4	21 52 24.301	02 23 26.39	18.10±0.07	1.79±0.21	0.96±0.14	G	17.2
FS29-5	21 52 25.420	02 23 39.32	14.75±0.02	0.65±0.03	0.11±0.02	S	20.0
FS29-6	21 52 26.697	02 23 20.29	19.81±0.18	1.60±0.51	1.20±0.42	G	20.1
FS29-7	21 52 25.200	02 22 57.37	19.74±0.18	0.34±0.33	−0.07±0.29	G	22.1
FS29-8	21 52 23.848	02 23 09.88	19.59±0.16	1.11±0.44	0.53±0.35	G	24.4
FS29-9	21 52 24.088	02 23 03.60	20.08±0.22	≥1.18	0.60±0.46	G	24.6
FS31-1	23 12 21.653	10 47 05.06	14.17±0.01	−0.23±0.01	−0.10±0.01	S	0.0
FS31-2	23 12 20.987	10 47 05.85	19.29±0.14	1.07±0.25	0.19±0.18	G	9.8
FS31-3	23 12 22.614	10 47 05.77	18.82±0.11	0.62±0.16	0.11±0.14	S	14.3
FS31-4	23 12 22.758	10 47 12.94	19.06±0.12	1.25±0.26	0.48±0.20	G	18.1
FS31-5	23 12 22.593	10 46 52.65	19.61±0.16	1.62±0.48	0.62±0.35	G	18.6
FS31-6	23 12 21.591	10 47 25.34	20.12±0.22	≥1.75	1.39±0.52	G	20.3
FS32-1	23 16 12.400	−01 50 34.70	13.81±0.01	−0.19±0.01	−0.09±0.01	S	0.0
FS32-2	23 16 11.741	−01 50 22.81	19.90±0.23	≥1.94	≥1.35	G	15.8
FS32-3	23 16 12.661	−01 50 16.37	15.00±0.02	0.80±0.03	0.30±0.02	S	19.1
FS32-4	23 16 11.130	−01 50 28.41	20.03±0.25	0.77±0.29	−0.01±0.25	S	20.5
FS33-1	12 57 02.337	22 01 52.69	14.44±0.01	−0.21±0.02	−0.10±0.02	S	0.0
FS33-2	12 57 01.833	22 01 54.55	20.47±0.29	0.93±0.61	≥0.76	G	7.2
FS33-3	12 57 02.842	22 01 45.43	18.64±0.10	1.84±0.29	1.25±0.22	G	10.1
FS33-4	12 57 02.173	22 02 10.40	19.53±0.16	0.92±0.27	0.84±0.26	G	17.8
FS33-5	12 57 03.893	22 01 52.62	20.37±0.27	1.10±0.48	≥1.35	G	21.7
FS33-6	12 57 02.863	22 01 31.83	20.17±0.24	≥1.92	1.18±0.44	G	22.1
FS34-1	20 42 34.713	−20 04 35.62	13.15±0.01	−0.15±0.01	−0.07±0.01	S	0.0
FS34-2	20 42 34.019	−20 04 32.30	18.54±0.10	2.41±0.37	1.70±0.26	G	10.2
FS34-3	20 42 35.042	−20 04 25.66	18.91±0.13	1.76±0.34	1.14±0.25	G	11.0
FS34-4	20 42 35.427	−20 04 42.50	19.54±0.19	≥1.64	≥2.71	G	12.3
FS34-5	20 42 35.832	−20 04 37.38	18.73±0.11	2.21±0.42	1.36±0.29	G	15.9
FS34-6	20 42 34.603	−20 04 54.71	19.90±0.24	0.72±0.45	0.60±0.47	G	19.1
FS34-7	20 42 33.367	−20 04 31.43	19.15±0.14	0.98±0.26	0.48±0.22	G	19.3
FS34-8	20 42 35.564	−20 04 19.87	18.07±0.08	2.06±0.26	1.10±0.16	G	19.8
FS34-9	20 42 34.994	−20 04 57.02	19.85±0.23	1.06±0.40	0.79±0.38	G	21.8
FS34-10	20 42 33.470	−20 04 51.34	19.01±0.13	1.16±0.26	0.68±0.21	G	23.4
FS127-1	10 06 28.916	41 01 24.97	11.85±0.00	0.30±0.01	0.04±0.01	S	0.0
FS127-2	10 06 27.378	41 01 17.66	20.37±0.31	1.57±0.53	0.85±0.56	G	18.8
FS131-1	12 14 25.403	35 35 54.42	11.51±0.00	0.29±0.01	0.03±0.01	S	0.0
FS131-2	12 14 24.421	35 36 01.85	19.41±0.18	1.51±0.33	1.41±0.38	G	14.0
FS131-3	12 14 26.001	35 36 14.32	18.37±0.09	1.73±0.25	1.14±0.22	G	21.2